Cross Delay Line Detectors for High Time Resolution Astronomical Polarimetry and Biological Fluorescence Imaging

O. Siegmund[1], J. Vallerga[1], P. Jelinsky[1], X. Michalet[2], and S. Weiss[2]

Abstract-- Ground based high time resolution astronomical polarimetry, imaging, and biological time-resolved molecular fluorescence lifetime imaging require specialized detectors. Photon counting detectors that combine high spatial resolution imaging with fast event timing capability for these uses have been a significant technical challenge. We have developed a high-temporal and spatial resolution, high-throughput sealed tube microchannel plate detector with electronic readout as tool for these applications. The design is based on a 25 mm diameter S20 photocathode followed by a microchannel plate stack, read out by a cross delay line anode with timing and imaging electronics. The detector supports 500 kHz global count rate, 10 kHz local count rate, 100 ps timing resolution and 40 μm spatial resolution. We describe the performance of the detector, as well as imaging results obtained with quantum dots and live cells.

***Index Terms*—Position sensitive photon detectors, Imaging, Time resolution, Polarimetry, Fluorescence lifetime imaging.**

I. Introduction

We have used the cross delay line anode [1]-[3] in a number of microchannel plate (MCP) detectors for spaceflight imaging and spectroscopy missions. The motivation for our current detector development stems from the described advances in the field of biological single molecule fluorescence, which faces the limitations of current detectors [4]-[10]. The cross delay line detector could open new windows in (i) multi-parameter studies of single molecules (simultaneous acquisition of lifetime, fluorescence spectrum and polarization), (ii) time resolved wide-field imaging of *in vivo* cellular processes or *in vitro* enzymatic reactions and (iii) high-throughput fluorescence correlation spectroscopy. In addition, the detector would fill the need for a high-temporal resolution imaging device in the field of single molecule enzymology and conformational dynamics. Time resolved wide-field imaging could be used for digital gating of fluorescence in living cells, allowing for a clear distinction between short-lived background autofluorescence and long-lived emission of fluorophores such as fluorescent semiconductor nanocrystals and quantum dots.

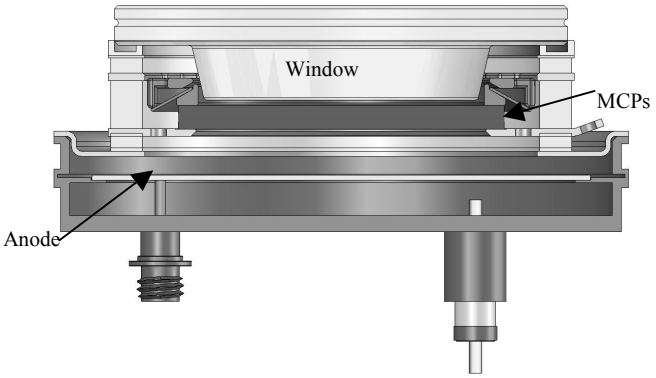

Fig. 1. Cross sectional view of the cross delay line photon counting, imaging microchannel plate sealed tube detector. Incoming photons pass through the fused silica window and are converted to photo-electrons by the S20 photocathode on the inner window surface. These are proximity focused onto the first of a set of three MCPs stacked in a back to back Z configuration. Upon amplification in the MCP stack (gain ~5 x 10^6) the charge cloud impinges onto a 29 mm^2 cross delay line anode for event position encoding.

Our detector system will also soon be employed for astronomical high time resolution investigations. With enough photons and temporal resolution, it is possible to investigate very small emission regions in great detail using light travel time causality consideration [11]. When coupled to the additional diagnostic tool of polarization, whose angle and degree constrains the geometry of the local magnetic field, it is thus possible to investigate the restricted emission zone geometry of a wide variety of astronomical objects such as pulsars, isolated neutron stars, gamma-ray bursters and the emitting regions of accretion disks associated with AGN and cataclysmic variable stars. This detector, with a polarimeter mounted on a large aperture ground-based telescope, will perform high-speed (μs) optical photo-polarimetry of all these types of objects. A major scientific goal is to use the detector to simultaneously measure all the Stoke's parameters of an incoming signal from an astronomical object by recording simultaneous position/time data for a set of polarimetric split images. Such instrumentation will be a trailblazer proto-type for future general-user high-speed detection devices that are

Manuscript received 11//11/2005

This work was supported by grants NASA #NAG5-11394, NIH 5 R21 RR017474

1. Experimental Astrophysics Group, Space Sciences Laboratory, University of California, Berkeley, California 94720, USA (e-mail: ossy@ssl.berkeley.edu).

1. Department of Chemistry & Biochemistry, University of California at Los Angeles, 607 Charles E. Young Drive E., Los Angeles, CA 90095, USA. (e-mail: michalet@chem.ucla.edu).

required to fully exploit the scientific potential of the next generation of extremely large aperture telescopes.

II. Detector Description

The implementation of a monolithic-ceramic cross delay line (XDL) detector in a sealed vacuum tube was first accomplished in our development of the GALEX mission MCP detectors [1] that are currently operating in-orbit. The basic configuration here is the same, however the anode and detector are specifically optimized for the high counting rates expected for the time resolved applications. We have employed a multi-alkali semitransparent proximity-focused photocathode (S20, Figs. 1, 2, 4) as the photo-conversion medium. A stack of three low resistance (25 MΩ) MCPs were used to accommodate high local event rates at modest gain (6 x 10^6). The XDL anode was designed with a cross-serpentine configuration (Fig. 3) to minimize the overall footprint and establish a fast propagation delay (20ns) appropriate for high global event rate capacity. All the materials used were metal or ceramic for compatibility with the ultra-high vacuum sealed tube configuration.

Fig. 2. Sealed tube detector inside its housing. High voltage and fast timing connections are radial, and the anode signals are positioned on the base.

The XDL anode was mounted in a vacuum header with SMA coaxial connectors for the anode signal outputs, and welded to a hermetic metal/ceramic brazed assembly that holds the MCPs. Verification tests were accomplished with the detector in an open vacuum tank prior to processing and sealing the detector. Processing consisted of a vacuum bakeout, high flux charge scrubbing of the MCP stack, followed by cathode deposition and final sealing of the tube. The seal method used was a hot indium seal between the window and the brazed assembly.

III. Test Results

A. Photocathode Efficiency

The photocathode that we have employed for our current development is a conventional S20 type multialkali. This was deposited onto the inside of the fused silica window using a standardized process, producing a quantum efficiency comparable with commercial S20 devices (Fig 4.). The background rate for this cathode was approximately 50 events/sec with the detector un-cooled. Since the counting rates of the planned tests were orders of magnitude above this level it was deemed unnecessary to use a cooler for the detector.

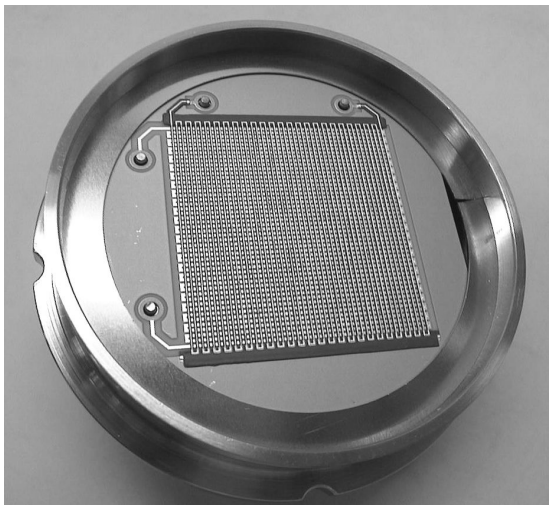

Fig. 3. 29 mm cross delay line anode installed into the base ring of the detector. The anode consists of a serpentine conductor for each axis, with a winding period of 0.6 mm, and the end to end delay produced is approximately 20 ns. Axes are isolated from each other by a refractory layer.

B. Electronic Position and Time Encoding Scheme

The electronic system for fast two dimensional imaging and timing is shown and described in Figs. 5 and 6. The position encoding for the cross delay line anode is based on encoding the arrival time differences of the event signals observed at the two ends of the delay lines. In this case we have taken the electronics developed for the SOHO [2] mission (Fig. 5) as our baseline system. Since this scheme was not configured for simultaneously recording the time of events, we have added a new circuit to accomplish coarse and fine time encoding for each event. The overall system for biological applications is shown in Fig. 6. The fast signal from the MCP output contact is amplified and used as the start signal for the Comtec 7072T time to digital converter. The stop signal is provided by the laser pulse trigger that initiates the events. In most cases the laser pulses do not result in any detected events, so having the MCP events trigger the start reduces the overall dead time of the system. The digitized time difference gives a ~15 ps fine time binning over a 50 ns time range. The laser pulses are also registered by a counter, and this number is also provided with the position and fine time as a course time measurement. To ensure that all the data belongs to the same event there is a coincidence circuit so if both the SOHO and 7072T have events within about 1 μSec the data is latched into the FIFO along with the current value in the counter, and then read out by the National Instuments DIO-32HS PCI card. The overall dead time is ~1.4 μs allowing rates of 500 kHz to be achieved with acceptable (<50%) deadtime losses. For the applications in astronomical polarimetry there is no laser pulse signal, so

the MCP output time signal is simply correlated to the local system clock to provide a time stamp (25ns accuracy) associated to each valid event.

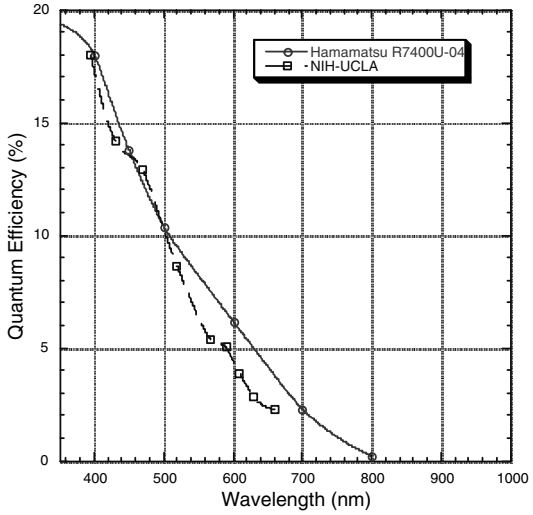

Fig. 4. Quantum detection efficiency for the detector S20 photocathode compared with a commercial S20 photocathode.

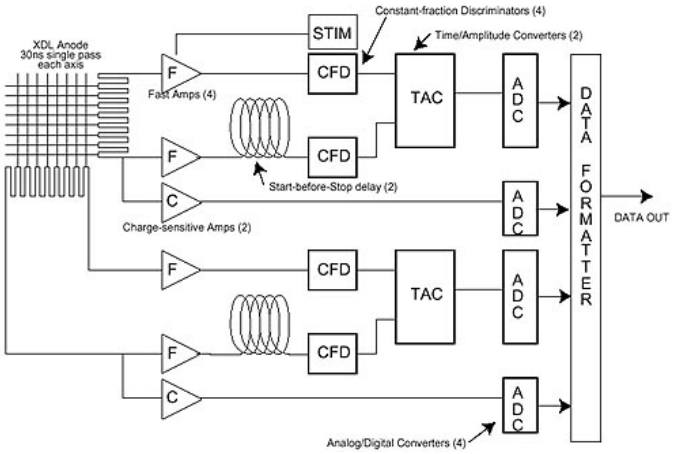

Fig. 5. Electronic processing chain for imaging with the cross delay line detector. Fast amplifiers on each delay line end amplify the signals, and one end of each delay line is delayed by slightly more than the overall delay of the anode. All fast signals are discriminated by constant fraction discriminators, and the output time differences are converted to analog values by a time to amplitude converter. Analog to digital conversion of the result gives a digital event centroid position for each axis. Charge signals are also amplified and digitized to monitor the overall gain of the detector.

C. Imaging and Timing Results

The detector was extensively tested under various conditions. The response of the sealed tube to uniform illumination is shown in Fig. 7. There is little fixed pattern noise, and no evidence of hexagonal structures that are often seen for MCPs due to the pore multi-fiber stacking structures. This is attributable to better MCP manufacturing processes established by Photonis recently. The edge enhancement is due to fringe fields resulting from the metal ring supporting the MCPs perturbing the field between the MCP stack and the XDL readout.

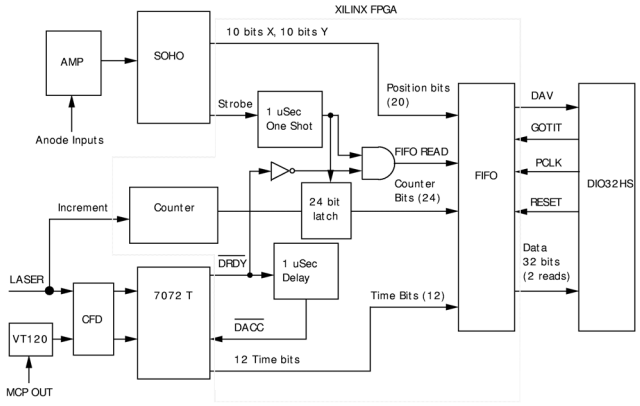

Fig. 6. Overall electronics scheme for the detector. Imaging data is processed by the amp and SOHO TDC as represented in Fig. 5, while the timing information is derived from the laser and the fast signal from the bottom contact of the MCP stack using a VT120 amplifier, constant fraction discriminator and Fast-Comtec 7072T TDC. Course timing information is provided by a counter, and position – time correlation is verified with a simple gate and delay logic. Data is buffed in a FIFO and then transferred to a National instruments DIO32HS PCI interface.

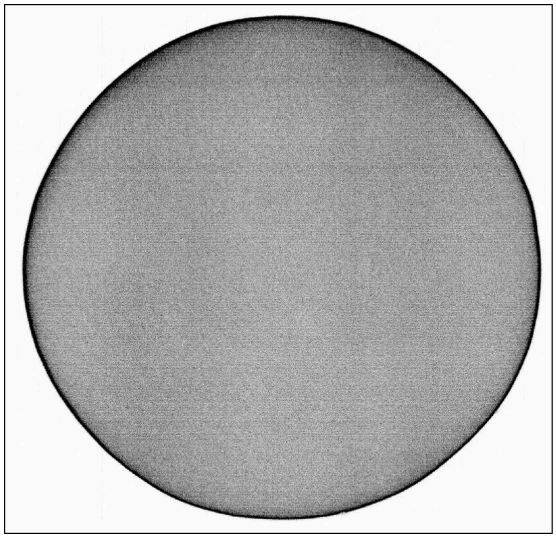

Fig. 7. Uniformly illuminated image using visible light, event rate 500 kHz, showing the uniformity of the response, and the lack of MCP multi-fiber modulation.

Resolution tests were performed both before and after the detector was sealed. Images of pinhole mask arrays (Fig. 8) allow both the point spread function and image linearity to be evaluated. The average width distributions of the pinhole images were measured as a function of MCP gain (Fig. 9) demonstrating that the resolution is better than 40 μm at modest gain (8 x 10^6). The resolution of the completed tube was measured by focusing a small spot (<50 μm) onto the cathode. This gave a ~80-90 μm image, showing that the proximity focus spread from cathode to MCPs is dominating the final resolution performance. The linearity over the central portion of the image is good with <1 resolution element position distortion.

The stability of the image and the resolution at high counting rates was also assessed. Uniformly illuminated images taken at 10 kHz, and 450 kHz showed no significant differences, and local spot images (90 µm spot) did not change position or width up to rates of 10 kHz in the spot (~100 events pore^{-1} sec^{-1}).

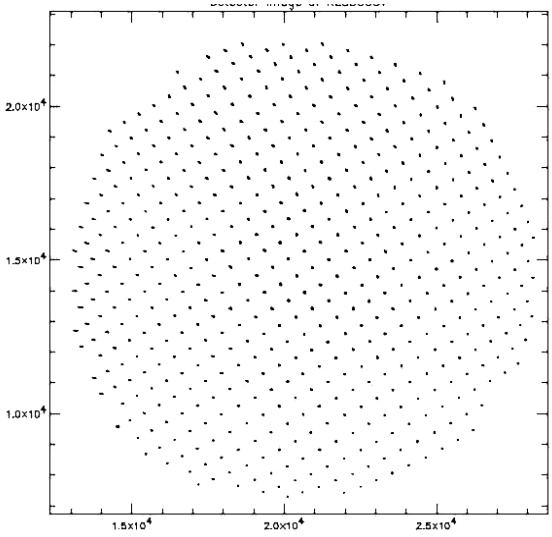

Fig. 8. Pinhole mask image taken before the final tube seal. A thin mask is in contact with the top MCP with 1mm hole spacing, and 10 µm hole width.

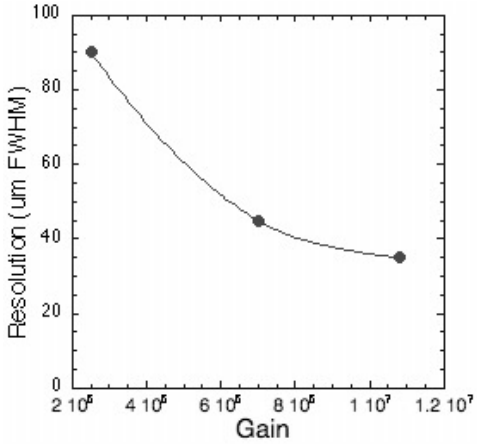

Fig. 9. The measured average width of the mask pinhole images shown in Fig. 8 for various gain MCP settings. This resolution is dominated by the electronics timing errors. The resolution of the final tube is closer to 80 µm FWHM due primarily to the large window to MCP proximity gap (~600 µm) causing photoelectron spread. A smaller proximity gap (<250 µm) can be achieved, but was not necessary for the current application.

D. Timing Results

The timing accuracy of the entire system was evaluated by illuminating the detector with a fast pulsed laser and measuring the difference between the laser trigger and the fast MCP pulse signal (Fig. 6). The overall timing jitter was ~100 ps FWHM as compared to the trigger jitter of the laser which is specified to be ~80 ps FWHM. The transit time spread for this type of detector due to the photoelectron trajectory spread in the proximity gap and MCP stack is of the order 25ps, so the main contribution to the system jitter is provided by the timing electronics.

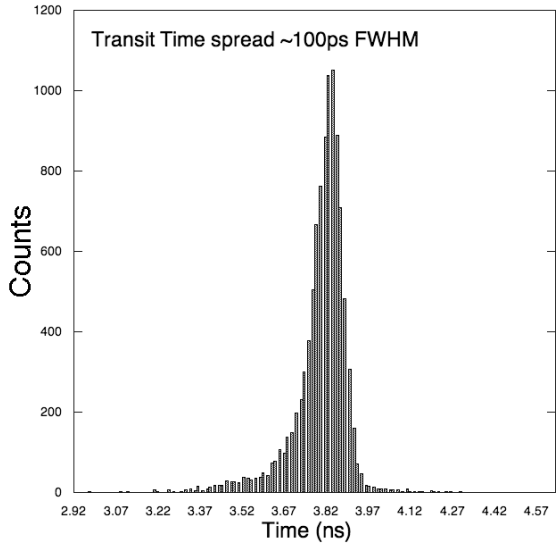

Fig. 10. Measured transit time spread of events using a pulsed laser with ~80ps jitter produced by comparing the laser trigger with the MCP output fast pulse (Fig. 6). The detector system jitter is probably better than 80 ps FWHM and is controlled by the electronics jitter, the proximity gap and MCP transit time spread.

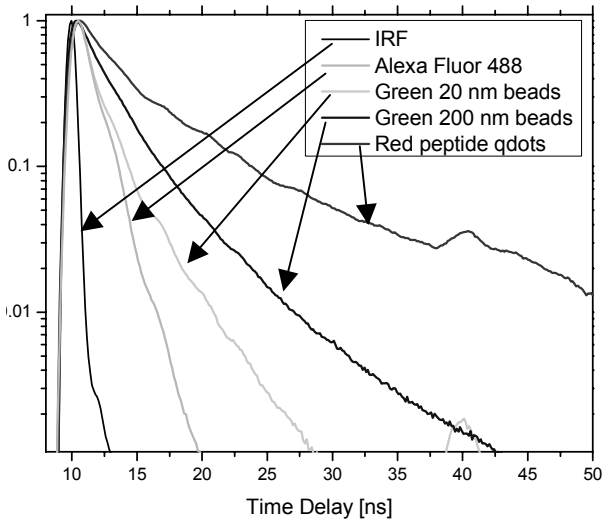

Fig. 11. Experimentally measured fluorescence decays of several characteristic samples. Dashed line: instrument response function (IRF) as determined by the 80 ps fluorescence decay of Erythrosin B in water. Alexa Fluor 488 nm in deionized water, measured lifetime: 1.26 ns; 20 nm yellow-green FluoSpheres (1.00 ns, 2.90 ns); 200 nm yellow-green FluoSpheres: (2.08 ns, 5.50 ns); Red peptide-coated quantum dots:(2.75 ns, 11.91 ns).

E. Biological Imaging and Timing Tests

Several tests of the detector system have been undertaken to specifically assess its capacity to image fluorescent samples, while simultaneously providing high-resolution temporal information on fluorescence lifetimes. Samples characterized by known fluorescence lifetimes were imaged as thin layers of liquid between glass cover-slips. Histograms of the time delay between each individual photon and the laser pulse provided a fluorescence decay curve convolved with the response function

of the instrument. Fig. 11 shows the results obtained with an organic dye molecule, fluorescent beads and quantum dots. The long lifetime of the quantum dots is distinguishable from the shorter lifetimes of the Alexa Fluor 488 dye and the dyes filling the fluorescent beads. Decay curve fits give lifetime values in agreement with the known lifetime components of these species.

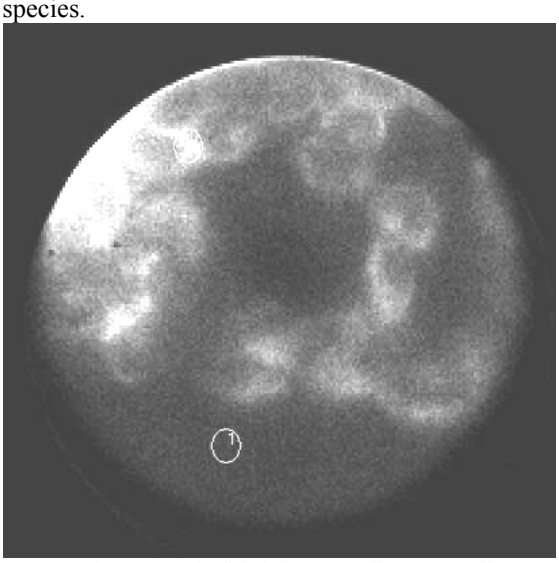

Fig. 12. Image of quantum dot labeled HeLa cells. HeLa cells expressing a chimeric avidin-CD14 fusion receptor on the exterior of their plasma membrane were incubated briefly with biotin-modified peptide-coated quantum dots. After rinsing away free quantum dots, the cells were observed in epifluorescence. Labeled receptors accumulate on the cell surface, but can also be recycled inside the cell over longer period of time. Image obtained with 340 s integration time (175 kHz count rate).

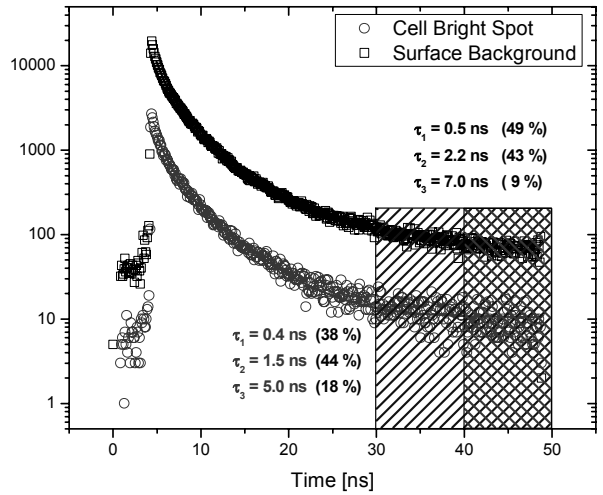

Fig. 13. Photon arrival time histogram for a region of interest located in one cell, and from a background area as defined in Fig 13. The time tagged photon list data acquisition allows events to be rebinned in time and/or position after recording to isolate any time period or position without constraining the dataset.

We then tested the time-stamping capabilities of the detector using live HeLa cells expressing chimeric surface receptors fused with avidin, detected with green biotinylated quantum dots. Fig. 12 shows a raw intensity image of the sample including all detected photons. The time decay curve of two selected regions is shown in Fig. 13 demonstrating the ability to simultaneously record position and time data for later analysis. We have also been able to image individual quantum dots (Fig.14) under CW laser excitation, demonstrating the spatial fidelity of the system.

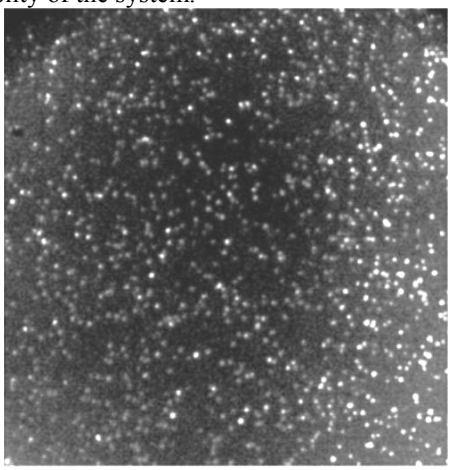

Fig. 14. 2 nM streptavidin coated quantum dots emitting at 565 nm on a glass coverslip. The 488 nm line (3.2 mW) of a continuous wave Argon ion laser was used to illuminate through the x60 objective lens of an inverted microscope. Total acquisition time: ~4 min. Image dimension 130 µm. Each spot corresponds to a single quantum dot point spread function.

IV. Acknowledgments

We thank F.F. Pinaud, J.M. Tsay and Drs. J.J. Li and G. Iyer for providing fluorescent samples and cells and J. Malloy, C. Scholz, Drs A. Tremsin and B. Welsh for their contributions to the detector development.

V. References

[1] O.H.W. Siegmund, P. Jelinsky, S. Jelinsky, J. Stock, J. Hull, D. Doliber, J. Zaninovich, A.S. Tremsin and K. Kromer, Proc. SPIE 3765 (1999) 429.
[2] O.H.W. Siegmund, M.A. Gummin, J. Stock, D. Marsh, R. Raffanti, T. Sasseen, J. Tom, B. Welsh, G. Gaines, P. Jelinsky, and J. Hull, *Proc. SPIE*, 2280 (1994) 89.
[3] O. H. W. Siegmund, Proc. SPIE . 4854 (2003) 181
[4] S. Weiss, Science 283 (1999) 1676.
[5] S. E. D. Webb, Y. Gu, S. Leveque-Fort, J. Siegel, M. J. Cole, K. Dowling, R. Jones, P. M. W. French, M. A. A. Neil, R. Juskaitis, L. O. D. Sucharov, T. Wilson, M. J. Lever, Rev. Sci. Instr. 73 (2002) 1898.
[6] O. Krichevsky, G. Bonnet, Rep. Prog. Phys. 65 (2002) 251.
[7] X. Michalet, F. F. Pinaud, L. A. Bentolila, J. M. Tsay, S. Doose, J. J. Li, G. Sundaresan, A. M. Wu, S. S. Gambhir, S. Weiss, Science 307 (2005) 538.
[8] L. A. Kelly, J. G. Trunk, K. Polewski, J. C. Sutherland, Rev. Sci. Instr. 66 (1995) 1496
[9] L. A. Kelly, J. G. Trunk, J. C. Sutherland, Rev. Sci. Instr. 68 (1997) 2279.
[10] V. Emiliani, D. Sanvitto, M. Tramier, T. Piolot, Z. Petrasek, K. Kemnitz, C. Durieux, M. Coppey-Moisan, Appl. Phys. Lett. 83 (2003) 2471.
[11] A. Shearer, and Golden, A., ApJ, 547 (2001) 967